Atmospheric
Chemistry
and Physics
Discussions

Open Access

ACPD

Interactive
comment

Interactive comment on "Tropical Pacific Climate Variability under Solar Geoengineering: Impacts on ENSO Extremes" *by* Abdul Malik et al.

Abdul Malik et al.

abdul.malik@kaust.edu.sa

Received and published: 29 August 2020

In the revised manuscript, we have included a separate section (2.4) under the title "ENSO representation in HadCM3L" which discusses the HadCM3L capability to simulate ENSO diversity as described by Cai et al. (2018). We have added the following text in the revised manuscript:

Before employing HadCM3L for studying ENSO variability under $4\times CO_2$, and G1, we evaluate its piControl simulation against present-day observational data. There is a non-linear relationship between tropical Pacific SST and rainfall (Ham 2017), which can be diagnosed by Niño3 region rainfall skewness (Cai et al., 2014). Skewness is a measure of asymmetry around the mean of the distribution (see eq. S1). Positive

skewness means that in given data distribution, the tail of the distribution is spread out towards high positive values, and vice versa (Ghandi et al., 2016). The skewness criterion is used to exclude climate models simulating overly wet or dry conditions over the Niño3 region (Cai et al., 2017). During extreme El Niño events, the ITCZ moves equatorward, causing significant increases in rainfall (> 5 mm day-1) over the eastern equatorial Pacific that skews the statistical distribution of rainfall in the Niño3 region. Thus, for studying extreme ENSO events, the model should be capable of simulating Niño3 rainfall above 5 mm day-1 and Niño3 rainfall skewness of greater than 1 over the entire simulated period (see our Sect. 3.2.2, and Cai et al., 2014 and 2015b). With a Niño3 rainfall skewness of 2.06 for piControl, HadCM3L fulfils this criterion.

In addition, we evaluate the ENSO modelled by HadCM3L following a principal component (PC) approach suggested by Cai et al. (2018). Considering distinct eastern and central Pacific ENSO regimes based on Empirical Orthogonal Function (EOF) analysis, they found that climate models capable of reproducing present-day ENSO diversity show a robust increase in eastern Pacific ENSO amplitude in a greenhouse warming scenario. Specifically, the approach assumes that any ENSO event can be represented by performing EOF analysis on monthly SST anomalies and combining the first two principal patterns (Cai et al., 2018). The first two PCs time series, PC1 and PC2, show a non-linear relationship in observational datasets (Fig. S1m). Climate models that do not show such a non-linear relationship cannot satisfactorily reproduce ENSO diversity, and hence are not sufficiently skilful for studying ENSO properties (Cai et al., 2018). Here, we perform EOF analysis on quadratically detrended monthly SST and wind stress anomalies of ERA5 and piControl over a consistent period of 41-year. We evaluate HadCM3L's ability to simulate two distinct ENSO regimes and the non-linear relationship between the first two PCs, i.e., PC2(t) = α[PC1(t)]^2 + β[PC1(t)]^2 + γ (Fig. S1). From ERA5, α = -0.36 (statistically significant at 99 % confidence level, hereafter "cl") whereas in piControl α = -0.31 (99 % cl), which is same as the mean α = -0.31 value calculated by Cai et al. (2018) averaged over five reanalysis datasets. The 1st and 2nd EOF patterns of monthly SST and wind stress anomalies of piControl (Fig.

S1 b, e) are comparable with that of ERA5 (Fig. S1 a, d). EOF1 of piControl shows slightly stronger warm anomalies in the eastern equatorial Pacific, whereas negative anomalies over the western Pacific are slightly weaker compared to ERA5. In EOF1, the stronger wind stress anomalies occur to the west of the Niño3 region, which is a characteristic feature during the eastern Pacific El Niño events (see Kim and Jin 2011a). Compared to ERA5, the spatial pattern of warm eastern Pacific anomalies is slightly stretched westwards, and wind stress anomalies are relatively stronger over the equator and South Pacific Convergence Zone (SPCZ). The 2nd EOF, in both ERA5 and piControl, shows warm SST anomalies over the equatorial central Pacific Niño4 region. The variance distributions for ERA5 and HadCM3L match well for EOF1 (ERA5: 82 %, piContol: 90 %) whereas a large difference exist for EOF2 (ERA5: 18 %, piControl: 10 %).

The PCA is also useful for evaluating how well HadCM3L represents certain types of ENSO events. Eastern and central Pacific ENSO events can be described by an E-Index (PC1-PC2)/$\sqrt{2}$), which emphasizes maximum warm anomalies in the eastern Pacific region, and a C-Index (PC1+PC2)/$\sqrt{2}$) respectively, which focuses on maximum warm anomalies in the central Pacific (Cai et al., 2018). Here, we show the eastern Pacific (EP) Pattern (Fig. S1 g, h) and central Pacific (CP) pattern (Fig. S1 j, k) by linear regression of mean DJF E- and C-Index, respectively, onto mean DJF SST and wind stress anomalies. We find that model's EP and CP patterns agree reasonably well with that of ERA5. HadCM3L underestimates the E-index skewness (1.16) whereas overestimates the C-Index skewness (-0.89) compared to ERA5 (2.08 and -0.58 respectively) averaged over DJF. HadCM3L's performance averaged over the entire simulated period of piControl is also consistent with ERA5 (Fig. S1; α: -0.32, EOF1: 64 %, EOF2, 8%, E-index skewness: 1.30, C-index skewness: -0.42). In general, in HadCM3L, the contrast between the E- and C-index skewness over the entire simulated period is sufficient enough to differentiate relatively strong warm (cold) events in the eastern (central) equatorial Pacific compared to the central (eastern) equatorial Pacific. Finally, we also evaluated the hf and BJ feedbacks which, for piControl, are very similar to those of

ERA5 (Table S5-6).

We conclude that HadCM3L has a reasonable skill for studying long-term ENSO vari-
ability and its response to solar geoengineering. However, we also highlight the need
for and hope to motivate future modelling studies that will help identify model depen-
dencies in the ENSO response. ———————————————————————
Figure Caption

Figure S1. ENSO diversity and nonlinear relationship between PCs. First monthly
principal pattern, EOF1, for (a) ERA5 and (b, c) piControl. Second monthly principal
pattern, EOF2, for (d) ERA5 and (e, f) piControl. DJF EP pattern for (g) ERA5 and (h, i)
piControl. DJF CP pattern for (j) ERA5 and (k, l) piControl. The nonlinear relationship
between PC1 and PC2 for (m) ERA5 and (n, o) piControl. The blue box indicates the
Niño3 (Niño4) region in a-c, and g-I (d-f and j-l). The left and the middle panel shows
EOF analysis over the 41 years of ER5 (1979-2019) and piControl. The right panel
shows EOF analysis over 990-year of piControl.

————————————————————

Interactive comment on Atmos. Chem. Phys. Discuss., https://doi.org/10.5194/acp-2018-1312,
2019.
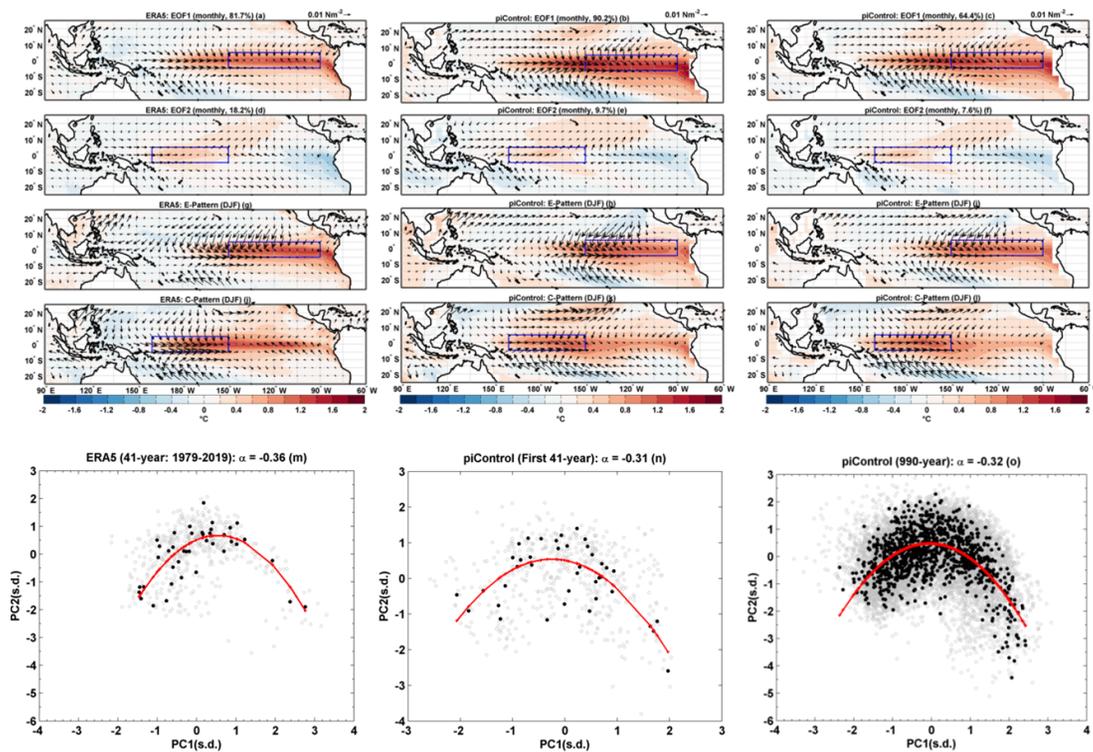
Fig. 1. Figure S1

Table S5. Mean DJF Heat Flux (hf) Feedback

Experiment	hf feedback or Damping Coefficient (Wm^{-2}/°C)	Difference w.r.t. piControl (Wm^{-2}/°C)	Std. Dev. 10,000 Realizations (Wm^{-2}/°C)	~ Change w.r.t. piControl (%)
ERA5	-14.59			
piControl	-14.70		0.52	
4×CO$_2$	-21.90	+7.19		+48*
G1	-14.85	+0.15		+1.0

*99% cl; **95% cl; Calculation period: ERA5 (41-yrs); HadCM3L (990-yrs)

Fig. 2. Table S5

Table S6. Mean DJF Bjerknes (BJ) Feedback

Experiment	BJ feedback (10^{-2} Nm^{-2}/°C)	Difference w.r.t. piControl (10^{-2} Nm^{-2}/°C)	Std. Dev. 10,000 Realizations (Wm^{-2}/°C)	~ Change w.r.t. piControl (%)
ERA5	3.3			
piControl	3.3		0.0091	
4×CO$_2$	2.2	-1.1		-33*
G1	3.5	+0.2		+6*

*99% cl; **95% cl; Calculation period: ERA5 (41-yrs); HadCM3L (990-yrs)

Fig. 3. Table S6